Article submitted to: High Power Laser Science and Engineering, 2025 *September 26, 2025*

Spatiotemporal characterization of pulse pedestals by imaging 2D Self-Referenced Spectral Interferometry

Thomas Oksenhendler[1,*], Stefan Bock[2,*], René Gebahrdt[2], Uwe Helbig[2], Yen-Yu Chang[2,4], Jörn Dreyer[2], Toma Toncian[2], and Ulrich Schramm[2,3]

[1]*iTEOX, Gometz-le-châtel, 91940, France*
[2]*Helmoltz-Zentrum Dresden-Rossendorf (HZDR), Bautzner Landstr. 400, Dresden, 01328, Germany*
[3]*Technische Universität Dresden, 01062, Dresden, Germany*
[4]*Amplitude, 2 rue du Bois Chaland, 91090, Lisses, France*
[*]*The authors contributed equally to this work.*

Abstract
The temporal contrast requirements for high-power laser pulses have become increasingly stringent with rising irradiance levels. Over the past decade, in addition to discrete pre-pulses, spatiotemporal pulse pedestals have attracted significant attention as a major limiting factor for contrast quality in chirped-pulse amplification s ystems, p rimarily c aused by imperfections in their stretching and compression optics. In this work, we present the first direct high-resolution single-shot measurement of these contributions in the spatiotemporal domain using an imaging spectrometer in combination with a two-dimensional self-referenced spectral interferometer.

Keywords: ultrashort laser pulses, metrology, CPA, high-intensity lasers

1. Introduction

Ultra-intense laser systems are employed in a broad range of applications in high-energy-density and relativistic laser–plasma physics. These research fields — enabled by the 2018 Nobel Prize awarded chirped pulse amplification (CPA) concept[1] — continuously drive the demand for higher peak intensities to access new regimes of experimental physics, including high-temperature plasma generation, ultra-compact particle acceleration, and even strong field quantum electrodynamic phenomena[2]. Recent large-scale ultrafast laser projects target peak powers on the order of 10 PW per pulse to achieve irradiances exceeding 10^{23} W/cm^2 at focus (see, e.g.[3,4]). At such intensities, temporal contrast ratios better than 10^{-12} together with absolute knowledge of the exact pulse shape are required on time scales ranging from nanoseconds to tens of picoseconds before the main pulse[5–9] for laser-plasma-interactions with solid state targets. Although various amplification techniques are employed, all systems rely on CPA[1] to mitigate optical damage and nonlinear effects during amplification and pulse shaping. CPA uses pulse stretchers and compressors to tailor the spectral phase, thereby increasing pulse duration and reducing peak power. These devices typically use diffraction gratings to geometrically disperse the pulse into its spectral components. However, surface imperfections on these optical elements directly affect the spectral phase of the pulse. As peak powers increase, so do the demands on temporal stretching and beam diameter, making the system more susceptible to spatiotemporal contrast degradation[10,11]. While spatiotemporal coupling is often discussed in the context of low-frequency components[10], which primarily affect the shape of the main pulse, contributions at higher temporal frequencies — extending to more than ten times the Fourier-limited pulse duration — are at least equally critical, as they lead to pre-plasma formation in the application[12]. Bromage et al. theoretically demonstrated that imperfections in stretcher and compressor optics can generate spatiotemporal pedestals with distinct slopes in both the temporal and far-field (k–t) domains[11]. These pedestals have been partially validated experimentally using third-order cross-correlators to probe temporal contrast in the near and far field[13,14] or a spatiotemporal cross-correlator on a specific experiment on stretcher-compressor apparatus[15]. However, a full high-resolution single-shot spatiotemporal characterization confirming these slopes experimentally at the output of a TW class laser system has not been achieved to date. In this work, we demonstrate that

Correspondence to: Email: thomas@iteox.com, Email: s.bock@hzdr.de

https://doi.org/10.1017/hpl.2025.10079 Published online by Cambridge University Press

spatiotemporal pedestals can be characterized using imaging spectrometry in combination with self-referenced two-dimensional spectral interferometry [16,17].

2. Experimental realization

An enhanced two-dimensional self-referenced spectral interferometry (2D SRSI) setup was implemented at the probe beam port of the CPA1 stage of the Draco laser system [17–19]. The port provides laser pulses of up to 10 mJ energy, centered around 800 nm, with a pulse duration of 30 fs and a repetition rate of 10 Hz. Here, 2 mJ at the entrance of the 2D SRSI device are used, in a beam with 5 mm full-width half-maximum spatial size are used.

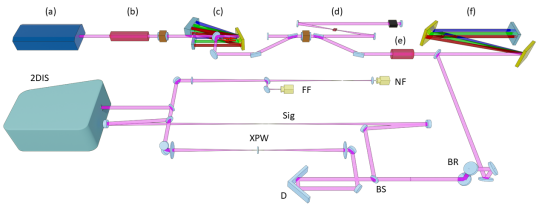

Figure 1. The oscillator (a) output is first amplified in a booster amplifier (b) and subsequently stretched in a classical Öffner stretcher (c). Further amplification and spectral pulse shaping are performed in a regenerative amplifier (d) and a multipass amplifier (e). The pulses are then compressed in an in-air compressor (f). A periscope (BR) rotates the pulse orientation by 90° to match the horizontal plane of the stretcher and compressor with the vertical slit of the spectrometer. In the 2D SRSI, a beamsplitter (BS) separates the light: the transmitted part is used to generate the reference (XPW) and the corresponding delay (D), while the reflected part is directed along the signal path (Sig) to the entrance slit of the imaging spectrometer (2DIS), where it is re-combined with the reference.

The 2D SRSI interferometer enables spatial–spectral interferometry by combining two pulses at the entrance slit of an imaging spectrometer (Princeton Instruments IsoPlane-320A), equipped with a 12-bit, 16-megapixel CMOS camera (ZWO ASI1600MM), as shown on figure 1. The reference pulse is self-generated from the signal pulse via a cross-polarized wave generation (XPW) [20,21], which provides a spatially, spectrally, and temporally clean reference, while the signal pulse remains undisturbed. Details of the 2D SRSI setup used can be found in [17], while the study of the SRSI method, its validity domain, algorithm, and limitations are described in [22].

To ensure consistent spatial orientation throughout the system, the pulse stretcher is first aligned to match the spatial dispersion plane of the air-based compressor. Subsequently, both stretcher and compressor are jointly matched to the vertical slit orientation of the imaging spectrometer. For this purpose, a periscope is positioned behind the compressor to rotate the beam such that the horizontal dispersion plane of the compressor and the stretcher aligns with the vertical spatial detection axis of the spectrometer.

The measured interferogram can be expressed as:

$$\widetilde{S}(x,\omega) = \widetilde{S_0}(x,\omega) + \widetilde{f}(x,\omega)e^{i(\omega\tau+k_x x)} + \widetilde{f}^*(x,\omega)e^{-i(\omega\tau+k_x x)}, \tag{1}$$

where the DC term is given by

$$\widetilde{S_0}(x,\omega) = \left|\widetilde{E}_{\mathrm{Ref}}(x,\omega)\right|^2 + \left|\widetilde{E}_{\mathrm{in}}(x,\omega)\right|^2, \tag{2}$$

the sum of the spectra of the XPW-filtered reference pulse $\left|\widetilde{E}_{\mathrm{Ref}}(x,\omega)\right|^2$ and the signal input pulse to be measured $\left|\widetilde{E}_{\mathrm{in}}(x,\omega)\right|^2$. The AC term is given by

$$\widetilde{f}(x,\omega) = \widetilde{E}^*_{\mathrm{Ref}}(x,\omega)\,\widetilde{E}_{\mathrm{in}}(x,\omega), \tag{3}$$

the interference of the two pulses. This formulation follows the principles of classical Fourier Transform Spectral Interferometry [20], with the distinction that the separation of AC and DC terms in the Fourier domain appears along the temporal axis and the spatial frequency axis in the temporal far-field k_x–t domain. This is illustrated in figure 2 by the intensity terms DC ($\widetilde{S_0}(x,\omega)$) and AC cross-correlation field term ($\widetilde{f}(x,\omega)$).

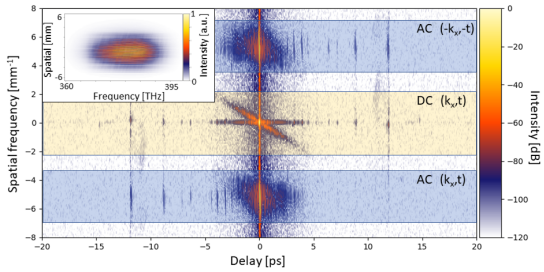

Figure 2. Temporal-far-field intensity in logarithmic scale of the interferogram. The spatio-spectral interferogram is shown in the inset.

The central term DC is centrosymmetric in the k_x-t domain. Since this symmetry is centered around the zero-frequency point, it already reveals the contribution of the pedestal along a diagonal line. Indeed, as theoretically predicted [11], in the time-domain far field, the pedestals arising from near-field contributions follow diagonal structures. In contrast, the contribution from the convex mirror of the employed Öffner stretcher, which is located in the far field, manifests as a pedestal aligned along the temporal axis. The corresponding far-field intensity in the time domain can be expressed in the form [11]:

https://doi.org/10.1017/hpl.2025.10079 Published online by Cambridge University Press

$$\langle I(k_x,k_y,t)\rangle = I_0(k_x,k_y,t) + \int_{-\infty}^{\infty} dt'\, I_0(k_x,k_y,t')\,\mathrm{PSD}_{\mathrm{cvx}}(t-t') + \sum_n \int_{-\infty}^{\infty}\int_{-\infty}^{\infty} du\,dv\, I_0(u,v,t+\gamma_n k_x-\gamma_n u)\,\mathrm{PSD}_n(k_x-u,k_y-v), \quad (4)$$

where I_0 denotes the far-field intensity of the pulse in the absence of spatiotemporal contributions, PSD_{cvx} is the power spectral density of the phase screen equivalent to the surface of the convex mirror, and PSD_n are the power spectral densities of the phase screens corresponding to near-field optics such as the concave mirror, diffraction gratings, or folding mirrors. The parameters γ_n are the spatio-spectral coupling coefficients (in mm/THz), which determine the central position of the beam on a given optical element as a function of the optical frequency ω by $x_n(\omega) = \gamma_n\omega$. In our configuration, the main contributions originate from two key optical components: the second, third grating (pass) and the roof mirror of the air compressor and the convex mirror of the Öffner stretcher. The contribution from the second and third grating (pass) and roof mirror is expected to appear along a diagonal in the k_x-t domain, with a slope of $-\frac{1}{\gamma} = -0.47\,\mathrm{mm}^{-1}/\mathrm{ps}$, resulting from the dispersion and setting of the compressor. In contrast, the contribution from the convex mirror, being a far-field optical element, is aligned along the temporal axis. Other contributions are expected with different slopes but at a much lower level due to the surface quality of their original optical component[11,14,15].

3. Results

In first place the expected characteristics in the k_x-t-space can be seen in the DC cross-correlation term. When using only one beam path (signal or reference) the DC^2 term represents an intensity autocorrelation in the far-field. Figure 3 shows the results for signal and XPW reference individually. The signal measurement clearly reveals the effects of optical imperfections introduced by the stretcher and compressor. In contrast, in the measurement of the reference the spatial-temporal structures are absent, due to the pulse cleaning of the XPW effect. Nevertheless, due to the autocorrelation-nature of the DC, phase information and potential asymmetric temporal shape are lost. The slope of the spatial-temporal tilted contribution is -0.47 mm^{-1}/ps, as expected. To reveal the phase information, as well as the temporal shape of the laser pulse, the signal and reference pulses have to be spatial-spectrally interfered in the 2D SRSI. Thus not only the DC terms are present in the k_x-t space, but also the AC term as cross correlation of signal and reference. The same contribution as in the DC appears on the AC term, but it is blurred by a slight defocusing between the two arms of the interferometer (figure 2). After subtracting this unintended defocusing contribution in the data post-treatment, the two signals AC^2 and DC show the pedestal on the same diagonal slope as shown on figure 4. The intensity profiles extracted from the DC term (figure 4 (a)) are symmetrical in time because they correspond to the sum of the autocorrelations of signal and reference. Whereas for the AC^2 term (figure 4 (b)), the cross-correlation between signal and references reveals the temporal (asymmetric) shape. The slope is identical for both terms and corresponds to the compressor parameters.

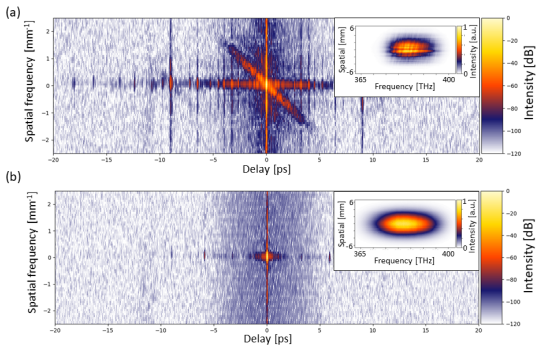

Figure 3. Temporal-far-field intensity in logarithmic scale of the spectrogram whose spatio-spectral intensity is shown in the inset, (a) for the signal and (b) for the XPW cleaned reference pulse.

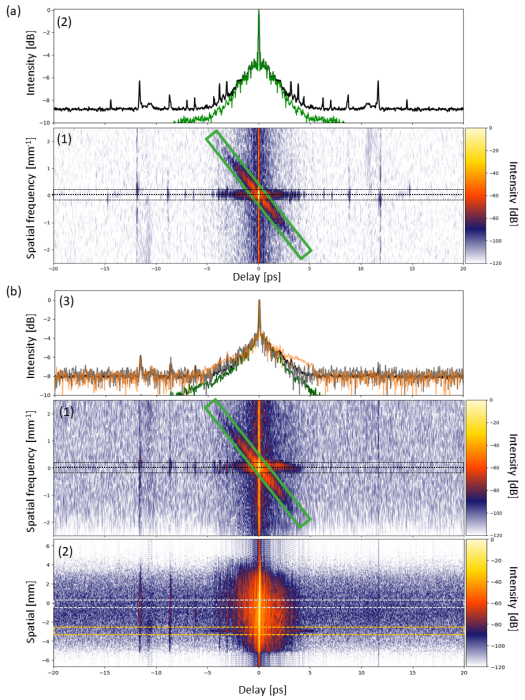

Figure 4. (a) (1) Temporal/far-field intensity in log scale of the interferogram for the DC term and the intensity profiles along the green box and black dotted line. (b) (1) Temporal/far-field intensity in log scale of the interferogram for the AC^2 term, (2) its temporal/near-field intensity and (3) the intensity profiles along the green box and black dotted line for the far field domain, and grey and orange for the central position and a lateral position showing a defect.

https://doi.org/10.1017/hpl.2025.10079 Published online by Cambridge University Press

In our case, the two contributions in the far-field are almost equivalent, as shown by the black and green curves in figure 4(b.3).

The inclined pedestal is generally not detected by third order cross-correlators measurering in the far field[23]. This type of device then only measures the pedestal along the temporal dimension, caused by the convex mirror in the stretcher.

Other third order cross-correlators[18,24] measure in the near-field instead, where the two contributions are almost indistinguishable because the inclination is small compared to the size of the beam; both contributions are overlapping. The spatiotemporal cross-correlation measurement[15] should be able to measure it, but it suffers from low temporal resolution (0.5 ps) and spatial frequency in far field (>0.2 mrad) despite the need to scan the spatial dimension. In addition, it has not yet been used to measure the spatiotemporal pedestal at the output of a TW-class laser beam. Here, we can derive a similar measurement as a near-field cross-correlator would result by Fourier-transforming the spatial frequency axis of the AC^2 term back to the spatial dimension. In our measurement by the 2D SRSI the spatial resolution reveals a local deterioration, as can be seen when comparing the temporal intensity profile at the central part of the near-field along the grey dotted box in figure 4 (b.2) in comparison to the profile along the orange region on the side of the near-field profile in figure 4(b.3). A typical near-field cross-correlator is detecting the total average of such a near-field profile.

Since, in our case, the dominant contribution comes from the convex mirror, the temporal intensity profiles are almost identical in the near- and far-field. Nevertheless, as the contribution of the compressor is fairly close, improving the surface quality of this mirror should only significantly increase the contrast in the far-field. Indeed, few improvements are expected in the near-field, which is also limited by the contributions of other optics, notably the second, third grating (pass) and roof mirror of the compressor.

4. Conclusion

In conclusion, the presented measurement results demonstrate the potential of 2D SRSI for capturing high-dynamic-range spatiotemporal features. Even a simpler measurement using only an imaging spectrometer provides access to the spatiotemporal intensity autocorrelation of the pedestal generated by the compressor grating. Both techniques operate in single-shot mode and can be implemented on large-scale ultrafast laser systems, where accurate characterization of such pedestals is essential. Since 2D SRSI measures the full electric field, a single acquisition allows for simultaneous evaluation of near-field and far-field contributions with high resolution and wide coverage in both spatial and temporal domains. This enables the identification of previously undetectable spatiotemporal distortions and facilitates the optimization of laser system performance. It is important to emphasize that the observed asymmetry in the far-field profile indicates that particular care must be taken in aligning the beam on the experimental target—especially in solid-state experiments. For spatiotemporally inclined pedestals, the incidence angle of the light on the target varies in time. As a result, the effective delay depends on the target angle, potentially leading to asymmetries in the pulse contrast. In high-contrast experiments, two opposite angles of incidence may thus produce significantly different temporal contrast profiles.

References

1. Donna Strickland and Gerard Mourou. Compression of amplified chirped optical pulses. *Optics Communications*, 56(3):219–221, 1985.
2. Félicie Albert, M E Couprie, Alexander Debus, Mike C Downer, Jérôme Faure, Alessandro Flacco, Leonida A Gizzi, Thomas Grismayer, Axel Huebl, Chan Joshi, M Labat, Wim P Leemans, Andreas R Maier, Stuart P D Mangles, Paul Mason, François Mathieu, Patric Muggli, Mamiko Nishiuchi, Jens Osterhoff, P P Rajeev, Ulrich Schramm, Jörg Schreiber, Alec G R Thomas, Jean-Luc Vay, Marija Vranic, and Karl Zeil. 2020 roadmap on plasma accelerators. *New Journal of Physics*, 23(3):031101, 2021.
3. M. O. Cernaianu, P. Ghenuche, F. Rotaru, L. Tudor, O. Chalus, C. Gheorghiu, D. C. Popescu, M. Gugiu, S. Balascuta, A. Magureanu, M. Tataru, V. Horny, B. Corobean, I. Dancus, A. Alincutei, T. Asavei, B. Diaconescu, L. Dinca, D. B. Dreghici, D. G. Ghita, C. Jalba, V. Leca, A. M. Lupu, V. Nastasa, F. Negoita, M. Patrascoiu, F. Schimbeschi, D. Stutman, C. Ticos, D. Ursescu, A. Arefiev, P. Tomassini, V. Malka, S. Gales, K. A. Tanaka, C. A. Ur, and D. Doria. Commissioning of the 1 pw experimental area at eli-np using a short focal parabolic mirror for proton acceleration. *Matter and Radiation at Extremes*, 10(2):027204, 2025.
4. Christophe Radier, Olivier Chalus, Mathilde Charbonneau, Shanjuhan Thambirajah, Guillaume Deschamps, Stephane David, Julien Barbe, Eric Etter, Guillaume Matras, Sandrine Ricaud, and et al. 10 pw peak power femtosecond laser pulses at eli-np. *High Power Laser Science and Engineering*, 10:e21, 2022.
5. V. Bagnoud and F. Wagner. Ultrahigh temporal contrast performance of the phelix petawatt facility. *High Power Laser Science and Engineering*, 4, 2016.
6. Tim Ziegler, Daniel Albach, Constantin Bernert, Stefan Assenbaum, Stefan Bock, Florian-Emanuel Brack, Thomas E. Cowan, Marco Garten, Nicholas P. Dover, Lennart Gaus, Rene Gebhardt, Ilja Goethel, Uwe Helbig, Arie Irman, Hiromitsu Kiriyama, Thomas Kluge, Akira Kon, Stephan Kraft, Florian Kroll, Markus Loeser, Josefine Metzkes-Ng, Mamiko Nishiuchi, Thomas Püschel, Lieselotte Obst-Huebl, Martin

https://doi.org/10.1017/hpl.2025.10079 Published online by Cambridge University Press

Rehwald, Hans-Peter Schlenvoigt, Ulrich Schramm, and Karl Zeil. Tproton beam quality enhancement by spectral phase control of a pw-class laser system. *Scientific Reports*, 11:7338, 2021.

7. Nicolas P. Dover, Tim Ziegler, Constantin Bernert, Stefan Assenbaum, Stefan Bock, Florian-Emanuel Brack, Thomas E. Cowan, Marco Garten, Emma J. Ditter, Lennart Gaus, Ilja Goethel, Hiromitsu Kiriyama, Thomas Kluge, James K. Koga, Akira Kon, Kotaro Kondo, Stephan Kraft, Florian Kroll, Hazel F. Lowe, Josefine Metzkes-Ng, Tatsuhiko Miyatake, Zulfikar Najmudin, Thomas Püschel, Martin Rehwald, Marvin Reimold, Hironao Sakaki, Hans-Peter Schlenvoigt, Keiichiro Shiokawa, Marvin E.P. Umlandt, Ulrich Schramm, Karl Zeil, and Mamiko Nishiuchi. Enhanced ion acceleration from transparency-driven foils demonstrated at two ultraintense laser facilities. *Light: Science & Applications*, 12:71, 2023.
8. Tim Ziegler, Ilja Göthel, Stefan Assenbaum, Constantin Bernert, Florian-Emanuel Brack, Thomas E. Cowan, Nicholas P. Dover, Lennart Gaus, Thomas Kluge, Stephan Kraft, Florian Kroll, Josefine Metzkes-Ng, Mamiko Nishiuchi, Irene Prencipe, Thomas Püschel, Martin Rehwald, Marvin Reimold, Hans-Peter Schlenvoigt, Marvin E.P. Umlandt, Milenko Vescovi, Ulrich Schramm, and Karl Zeil. Laser-driven proton acceleration beyond 100 mev by radiation pressure and coulomb repulsion in a conduction-restricted plasma. *Nature Physics*, 20:1211, 2024.
9. Yinren Shou, Xuezhi Wu, Ki Hong Pae, Gwang-Eun Ahn, Seung Yeon Kim, Seong Hoon Kim, Jin Woo Yoon, Jae Hee Sung, Seong Ku Lee, Zheng Gong, Xueqing Yan, Il Woo Choi, and Chang Hee Nam. Laser-driven proton acceleration beyond 100 mev by radiation pressure and coulomb repulsion in a conduction-restricted plasma. *Nature Communications*, 16:1487, 2025.
10. Spencer W Jolly, Olivier Gobert, and Fabien Quéré. Spatio-temporal characterization of ultrashort laser beams: a tutorial. *Journal of Optics*, 22(10):103501, 2020.
11. J. Bromage, C. Dorrer, and R. K. Jungquist. Temporal contrast degradation at the focus of ultrafast pulses from high-frequency spectral phase modulation. *Journal of the Optical Society of America B*, 29(5):1125, apr 2012.
12. Constantin Bernert, Stefan Assenbaum, Stefan Bock, Florian-Emanuel Brack, Thomas E. Cowan, Chandra B. Curry, Marco Garten, Lennart Gaus, Maxence Gauthier, René Gebhardt, Sebastian Göde, Siegfried H. Glenzer, Uwe Helbig, Thomas Kluge, Stephan Kraft, Florian Kroll, Lieselotte Obst-Huebl, Thomas Püschel, Martin Rehwald, Hans-Peter Schlenvoigt, Christopher Schoenwaelder, Ulrich Schramm, Franziska Treffert, Milenko Vescovi, Tim Ziegler, and Karl Zeil. Transient laser-induced breakdown of dielectrics in ultrarelativistic laser-solid interactions. *Physical Review Applied*, 19(1):014070, 2023.
13. Xiaoming Lu, Xinliang Wang, Yuxin Leng, Xiaoyang Guo, Yujie Peng, Yanyan Li, Yi Xu, Rongjie Xu, and Xinyuan Qi. Suppressing temporal pedestal in nd:glass laser systems by avoiding far-field spectral phase noise. *IEEE Journal of Selected Topics in Quantum Electronics*, 24(5):1–6, 2018.
14. Simon Roeder, Yannik Zobus, Zsuzsanna Major, and Vincent Bagnoud. Improving the rising edge of the temporal contrast of phelix by spatial conditioning in an unfolded stretcher. *Optics Express*, 32(20):35713, 2024.
15. Jingui Ma, Peng Yuan, Jing Wang, Yongzhi Wang, Guoqiang Xie, Heyuan Zhu, and Liejia Qian. Spatiotemporal noise characterization for chirped-pulse amplification systems. *Nature Communications*, 6:6192, 2015.
16. Thomas Oksenhendler, Pierre Bizouard, Olivier Albert, Stefan Bock, and Ulrich Schramm. High dynamic, high resolution and wide range single shot temporal pulse contrast measurement. *Optics Express*, 25(11):12588, 2017.
17. Thomas Oksenhendler, Stefan Bock, Jörn Dreyer, René Gebhardt, Uwe Helbig, Toma Toncian, and Ulrich Schramm. Advanced laser pulse metrology through 2d self-referenced spectral interferometry. *Scientific Reports*, 15(1), 2025.
18. S. Bock, Thomas Oksenhendler, Thomas Püschel, René Gebhardt, Uwe Helbig, Richard Pausch, Tim Ziegler, Constantin Bernert, Karl Zeil, Arie Irman, Toma Toncian, Hiromitsu Kiriyama, Mamiko Nishiuchi, Akira Kon, and Ulrich Schramm. Spectral-temporal measurement capabilities of third-order correlators. *Optics Express*, 31(6):9923, 2023.
19. Stefan Bock, Franziska Marie Herrmann, Thomas Püschel, Uwe Helbig, René Gebhardt, Jakob Johannes Lötfering, Richard Pausch, Karl Zeil, Tim Ziegler, Arie Irman, Thomas Oksenhendler, Akira Kon, Mamiko Nishuishi, Hiromitsu Kiriyama, Kiminori Kondo, Toma Toncian, and Ulrich Schramm. Characterization of accumulated b-integral of regenerative amplifier based CPA systems. *Crystals*, 10(9):847, 2020.
20. T. Oksenhendler, S. Coudreau, N. Forget, V. Crozatier, S. Grabielle, R. Herzog, O. Gobert, and D. Kaplan. Self-referenced spectral interferometry. *Applied Physics B*, 99(1-2):7–12, 2010.
21. A. Jullien, L. Canova, O. Albert, D. Boschetto, L. Antonucci, Y.-H. Cha, J.P. Rousseau, P. Chaudet, G. Chériaux, J. Etchepare, S. Kourtev, N. Minkovski, and S.M. Saltiel. Spectral broadening and pulse duration reduction during cross-polarized wave generation: influence of the quadratic spectral phase. *Applied Physics B*, 87(4):595–601, 2007.
22. Thomas Oksenhendler. Self-referenced spectral

https://doi.org/10.1017/hpl.2025.10079 Published online by Cambridge University Press

interferometry theory. *arXiv.1204.4949*, 2012.

23. V. A. Schanz, F. Wagner, M. Roth, and V. Bagnoud. Noise reduction in third order cross-correlation by angle optimization of the interacting beams. *Optics Express*, 25(8):9252, 2017.
24. S Luan, M H R Hutchinson, R A Smith, and F Zhou. High dynamic range third-order correlation measurement of picosecond laser pulse shapes. *Measurement Science and Technology*, 4(12):1426–1429, 1993.

https://doi.org/10.1017/hpl.2025.10079 Published online by Cambridge University Press